Performance of the pn-EPIC Detector aboard XMM

Martin Popp[1*], Robert Hartmann[1], Lothar Strüder[1], Heike Soltau[2], Peter Holl[2],
Norbert Meidinger[1], Ulrich Briel[1], Eckart Kendziorra[3], Markus Kuster[3]

[1]Max-Planck-Institut für extraterrestrische Physik, Giessenbachstr., D-85740 Garching, Germany
[2]KETEK GmbH, Am Isarbach 30, D-85764 Oberschleissheim, Germany
[3]Institut für Astronomie und Astrophysik der Universität Tübingen Abteilung Astronomie,
Waldhäuser Strae 64, D-72076 Tübingen, Germany

[*]*Corresponding author, mailing address: MPI Halbleiterlabor,*
Paul-Gerhardt-Allee 42, D-81245 München, Germany
Telephone: +49 (89) 839400 - 44; Fax: +49 (89) 839400 -11
E-mail: mpo@mpe.mpg.de

ABSTRACT

One of the three imaging spectroscopic cameras abord XMM will be equipped with a pn-CCD. The chip exhibits features that make it ideally suited for the XMM mission. Due to its layout, quantum efficiency is very good, especially at very low and very high X-ray energies. Parallel signal preamplification makes fast readout possible, resulting in high time resolution of 70 ms for Full Frame readout or even a few μs for the timing mode, where only part of the CCD is read out. Radiation hardness has been tested and proven to be excellent.

The Flight Model camera has been calibrated at various test sites. An overview over the achieved performance is given in the following text.

1. Introduction

The pn-EPIC (European Photon Imaging Camera, [Bignami]) detector chip is a CCD which has been developed at the Halbleiterlabor der Max-Planck Institute für Physik und extraterrestrische Physik. The camera will be placed at the focus of the telescope module that is not obscured by the RGA box of the Reflection Grating Spectrometer, thus having the highest effective area of the three EPIC detectors. It consists of an array of 12 identical subsystems of 12800 pixels each that are monolitically integrated on one wafer. The large pixel size of $150\mu m \times 150\mu m$, corresponding to 4.1 arc sec resolution, is well adapted to the performance of the Wolter telescope and, together with parallel signal preamplification, results in a very fast readout of the chip. The layout of the chip makes a full depletion of the device possible rendering the whole thickness of $280\mu m$ sensitive to X-rays. It is therefore ideal for the detection of X-rays in the band up to 10 keV. Because there is no field free region, the chip can be back-illuminated and the backside entrance window is optimized for detection of low energy photons down to 200 eV.

For a detailed description of the layout and production of the chips, see e.g. [Holl]. Flight model prototypes have been tested in the MPE-Panter test facility (Munich), in the IAS Jupiter test facility at Orsay and in the PTB laboratory at the BESSY synchrotron ring in Berlin. Preliminary results of the calibration are presented in [Briel].

2. Quantum Efficiency

Quantum efficiency (QE) measurements have been performed with flight type test devices at the BESSY Synchrotron facility at Berlin. Calibration of the Flight model has been done at the IAS facility at Orsay [Dhez]. For energies below 1500 eV, a grating monochromator has been used in the SACO synchrotron beamline while for the energies up to more than 10 keV, a double crystal monochromator at the DCI - Beamline has been used.

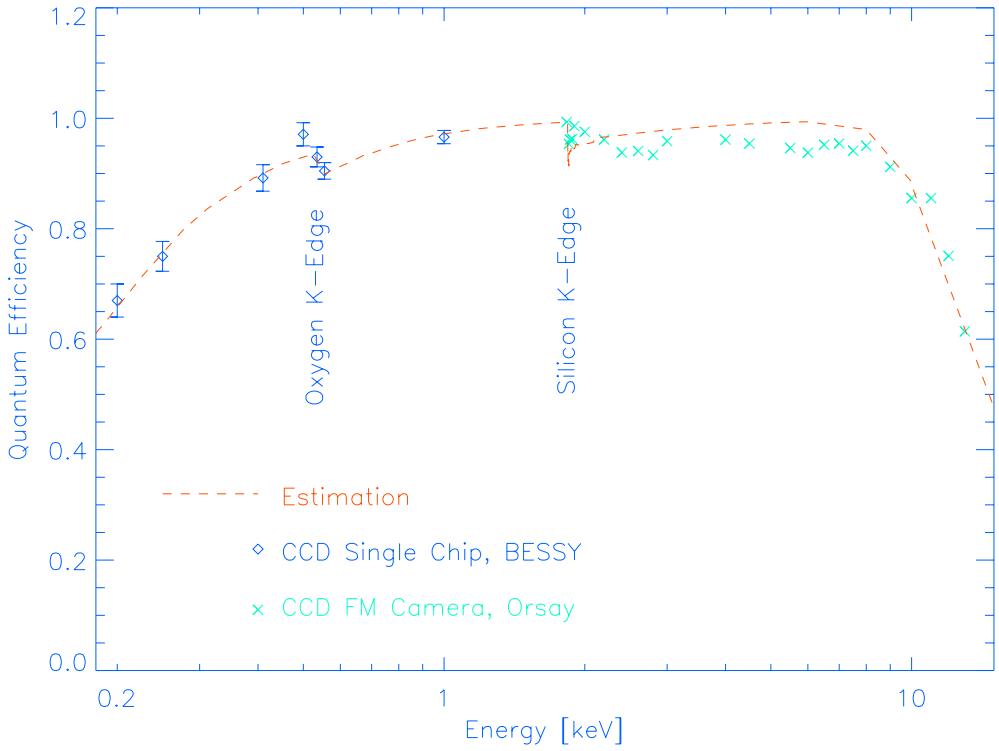

Fig. 1.— Quantum efficiency of the pn-CCD: the measurements are in good agreement with modelled data. The effect of the absorption edges can be clearly seen. The data marked by rhombs has been taken with Flight Model-like test devices, so-called Single Chips

Preliminary results are shown in Fig. 1. All the data taken at the different beamlines are in good agreement with the model estimation. One can clearly see the effect of absorption edges at O-K and Si-K, but the drop in efficiency is only about 5% for each edge. Due to the absence of

nitride on the entrance window, no edge effect is observed around 400 eV. The optimized ultra-thin entrance window [Hartmann(1),Hartmann(2)] ensures good QE even at very low energies. Because the entrance window is free of lithographic structures in contrast to a front illuminated device, the X-ray response and the QE are homogeneous over the whole sensitive area.

3. Spectral Response

At medium and higher energies ($\geq 2keV$), the response to monoenergetic X-rays is approximately given by a gaussian with a width that is dominated by the sum of the noise contributions due to the statistical fluctuations of charge generation (Fano - noise), electronic noise of the readout, which is about $5.0e^-$ (rms) equivalent noise charge and a small contribution due to charge transfer losses, which only becomes important for energies above 2 keV. The values achieved during calibration measurements with the Flight Model at the MPE - Panter test facility in Neuried/Munich are shown in Fig 2. The FWHM is 145 eV at 6.4 keV and 70 eV at 500 eV.

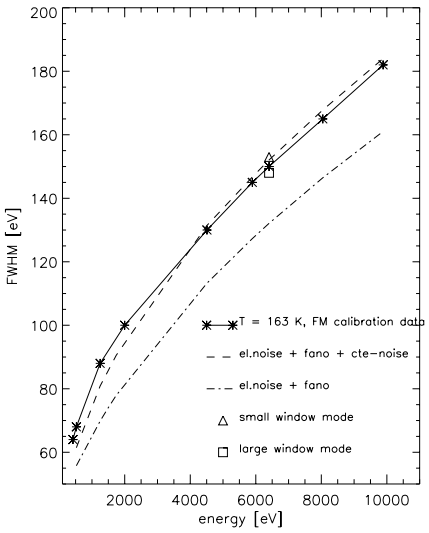

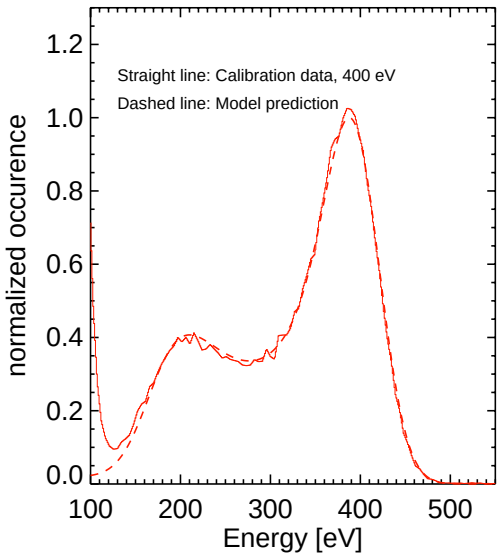

Fig. 2.— Values of FWHM for monochromatic line spectra achieved during calibration measurements: the deviation of the data from the theoretical limit (dash-dotted line) is explained by noise due to statistical fluctuations of charge loss (CTE - noise).

Fig. 3.— Example of response to synchrotron radiation of 400 eV, together with model prediction

At lower energies, partial events become more important. These are accounted for by a dedicated analytical model [Hartmann(2), Popp]. The observed effects can be modelled by introduction of a partially sensitive layer on top of the detector entrance window. An example is shown in Fig 3. This model will be used to build up the response matrix in the data analysis package.

4. Operating Modes

The detector can be operated in three imaging and two timing modes. In timing mode, the spatial information in one (row-) dimension is discarded due to continous readout without integration time. Readout of the whole detector in Full Frame Mode is done within 70 ms with a ratio of integration to readout time of 11:1, so that there are only 7% out of time events. These events are due to photons that are absorbed during the readout, so that their apparent (row-) position is wrong. In timing mode, the time resolution is of the order of $30\mu sec$ with uninterrupted observation of the target. In Burst mode, the time resolution reaches $7\mu sec$, but the duty cycle is significantly less than 100 %. Even very bright point sources (up to 6.3 Crab) can be observed without pile-up. A summary of the relevant parameters is given in the table. An example of a lightcurve analysis is given in Fig. 4. A pulsating source has been simulated by means of a rotating chopper wheel in front of a X-ray tube, resulting in a sinusodial variation of the X-ray flux with time. The period for the measurement shown was fixed to 5.12 ms. More details are given in [Kendziorra].

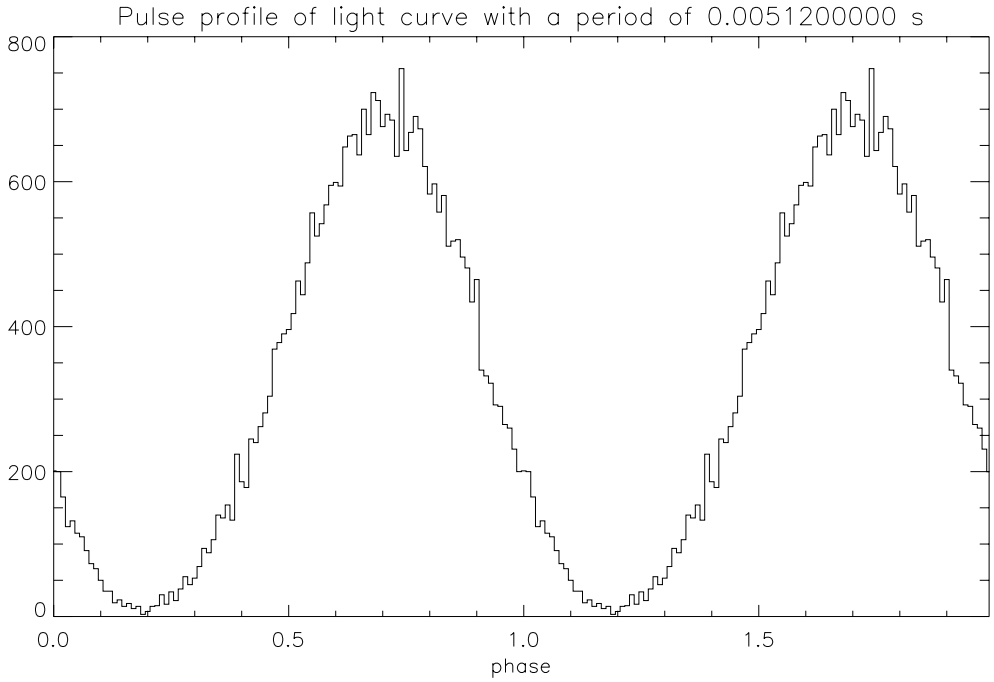

Fig. 4.— Light curve of a pulsating source, simulated with a chopper wheel at the Panter test facility. The period can be determined with a relative error of less than 10^{-4}

Mode	**Field of view** *in arc min*	**Integration time** *in msec*	**Transfer time** *in msec*	**Readout time / CCD** *in msec*	**Frame Time** *in msec*	**Out of time events** *in %*	**Duty cycle** *in msec*	**Brighest point source for XMM** *in mCrab*
Full Frame 400 × 384 pixel	27.5 × 26.4	65.3	N.A.	4.654	70.3	7	100	0.7
ext. Full Frame (5 wait states)	27.5 × 26.4	275	N.A.	4.654	280	2	100	obs. of extended sources
Small window (64 × 64 pixel)	4.4 × 4.4	4.0	0.098	1.52	5.7	2	71	11
Large Window 200 × 384 pixel	13.8 × 26.4	42.0	0.072	2.494	44.6	0.3	91	1.1
Timing $150 \times 1500 \mu m^2$ pixel	4.4 × 13.8	0.03	N.A.	N. A.	5.9	all	98.5	146
Burst (180 lines read)	4.4 × 1.4	0.007	N.A.	4.195	4.3	all	0.17	6300

5. Radiation Hardness

During operation in orbit, the detector will also be exposed to irradiation with high energy particles, mainly protons. The main effect of radiation damage is a degradation of the charge transfer efficiency [Meidinger].

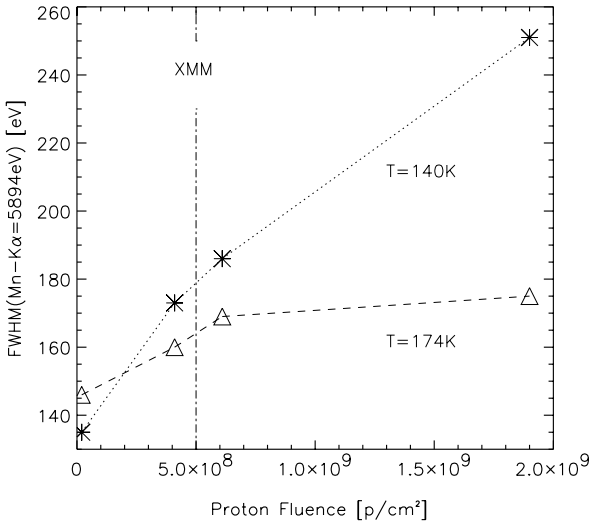

Fig. 5.— Change of FWHM with irradiation dose: For higher doses (i.e. later in the operation cycle), the temperature of the detector can be optimized. The vertical dash-dotted line designates the expected dose after 10 years of operation in orbit. Note that the test results are shown up to a factor 4 of that value.

This has to be accounted for by continous in-orbit calibration of this parameter, which can be done with the on-board calibration source. Test measurements on radiation damage have been conducted on flight type test CCDs, where the CCD's have been exposed to 10 MeV protons using the TANDEM accelerator at the Technische Universität München. No breakdown or failure of a device has been observed up to doses that correspond to several times the expected dose at end of mission. The resulting change in spectral resolution is shown in Fig. 5. It can be minimized by the optimization of the operation temperature. After an irradiation corresponding to 40 years of operation in space (four times the projected XMM mission duration), the FWHM is deteriorated by 20 % only.

6. Simulations

An analytical model has been developed to reproduce the spectral response of the pn-CCD. Details are described in [Popp]. Its parameters have been adjusted to the results of the calibration measurements. It accounts for the effects of non-unity QE as well as for incomplete charge collection near the surface of the entrance window. It can be used to simulate the response of the camera to any astronomical input spectrum. An example for a supernova remnant using a MEKAL model is shown in Fig. 6. Further work to extend the model, taking into account the influence of charge splitting, out-of-time events and pile-up is ongoing.

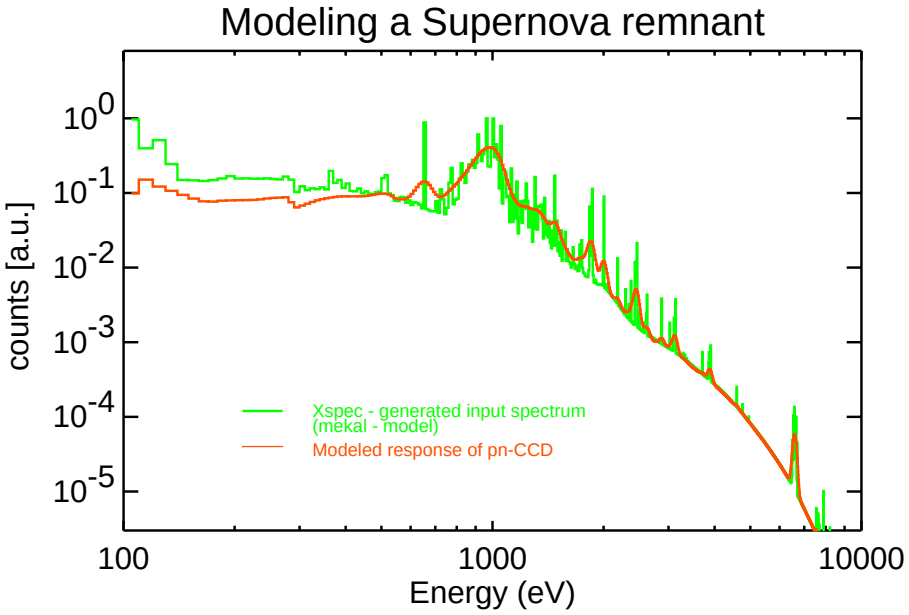

Fig. 6.— Simulation of a SNR spectrum (effective area of telescope and thin filter applied). The input was generated using the MEKAL model of the XSPEC package

Acknowledgments

We thank P. Solč for the mounting and bonding of the devices. We thank the staff at the semiconductor laboratory for its outstanding commitment during the production of the devices. The project was supported by the Deutsche Agentur für Raumfahrtangelegenheiten (DARA) under contract No. 50 OX 93025/-XMM-EPIC and by the European Space Agency under contract No. 8873/90/PB(SC) CCN No.1.

REFERENCES

Bignami, G.F. et al., European Photon Imaging Camera (EPIC) for X-Ray Astronomy, SPIE Vol.1344:144 - 153, (1990)

Briel, U. et al., Calibration and performance of the XMM EPIC PN camera: imaging modes, submitted to SPIE, 3445, (1998)

Dhez, P. et al., Institut d'Astrophysique spatiale (IAS) 0.1-15 keV Synchrotron Radiation Facility beam lines, SPIE, Vol. 3114:134-142, (1997)

Hartmann, R. et al., Ultrathin entrance windows for silicon drift detectors NIM A, 387:250 - 254, (1996)

Hartmann, R. et al., Low energy response of silicon pn-junction detectors, NIM A, 377(2,3):191 - 196, (1996)

Holl, P. et al., A $36cm^2$ Monolithic pn-CCD for X-ray Detection on the XMM and ABRIXAS Satellites, IEEE Trans. Nucl. Sci, 45(3) Part I: 931 - 935, (1998)

Kendziorra, E. et al., PN-CCD camera for XMM: performance of high time resolution/bright source operating modes, SPIE, 3114:155-165, (1997)

Meidinger, N. et al., Analysis of trapping effects on charge transfer in proton irradiated pn-CCDs, NIM A, 377(2,3):298 - 311, (1996)

Popp, M. et al., Modelling the energy response of pn-CCDs in the 0.2 - 10 keV band, submitted to NIM A (1998)